ZnSnSb 2 anode: A solid solution behavior enabling high rate capability in Li-ion batteries

Gaël Coquil, Bernard Fraisse, Stéphane Biscaglia, David Aymé-Perrot, Moulay Tahar Sougrati, Laure Monconduit

▶ **To cite this version:**

Gaël Coquil, Bernard Fraisse, Stéphane Biscaglia, David Aymé-Perrot, Moulay Tahar Sougrati, et al.. ZnSnSb 2 anode: A solid solution behavior enabling high rate capability in Li-ion batteries. Journal of Power Sources, 2019, 441, pp.227165. ⟨10.1016/j.jpowsour.2019.227165⟩. ⟨hal-03094895⟩

HAL Id: hal-03094895

https://hal.science/hal-03094895v1

Submitted on 4 Jan 2021

HAL is a multi-disciplinary open access archive for the deposit and dissemination of scientific research documents, whether they are published or not. The documents may come from teaching and research institutions in France or abroad, or from public or private research centers.

L'archive ouverte pluridisciplinaire **HAL**, est destinée au dépôt et à la diffusion de documents scientifiques de niveau recherche, publiés ou non, émanant des établissements d'enseignement et de recherche français ou étrangers, des laboratoires publics ou privés.

HAL Authorization

$ZnSnSb_2$ anode: A solid solution behavior enabling high rate capability in Li-ion batteries

Gaël Coquil[a], Bernard Fraisse[a], Stéphane Biscaglia[b], David Aymé-Perrot[c], Moulay T. Sougrati[ae] and Laure Monconduit[ad]

[a] Institut Charles Gerhardt – AIME, CNRS UMR 5253, Université de Montpellier CC 15-02, Pl. E. Bataillon, 34095 Montpellier, France
[b] ADEME – Département Energies Renouvelables, 500 route des Lucioles, 06560 Valbonne, France
[c] Direction R&D TOTAL S.A., Tour Michelet A, 24 Cours Michelet, La Défense 10, 92069 Paris-La Défense, France
[d] Réseau sur le Stockage Electrochimique de l'Energie (RS2E), CNRS FR3459, 33 Rue Saint Leu, 80039 Amiens, France

ABSTRACT

$ZnSnSb_2$ intermetallic alloy as anode material for Li-ion batteries has been investigated for the first time in this work. This material is able to deliver a high capacity of 615 mAh/g for 200 cycles at *4C* (a current density of 0.25 A/g) with a good a coulombic efficiency exceeding 99.3 %. Furthermore, the electrode material exhibit a high rate capability between *C/5* (12.6 mA/g) and *10C* (630 mA/g), with a reversible capacity loss of 19% and a polarization increasing of only 0.05 V. Among all reported MSnSb (with M= Ag, Ti, Cu…) alloys, $ZnSnSb_2$ exhibits the most outstanding rate capability and long cycling life. The observed behavior can be linked not only to the *quasi-topotactic* de/lithiation reaction between the $ZnSnSb_2$ and Li_3Sb but also to the solid solution mechanism evidenced from *operando* X-ray diffraction analysis. This suggests that the electrode exhibits a great resistance to the volume expansion and the mechanical stress during cycling even at high cycling rates (*10C*).

TOC

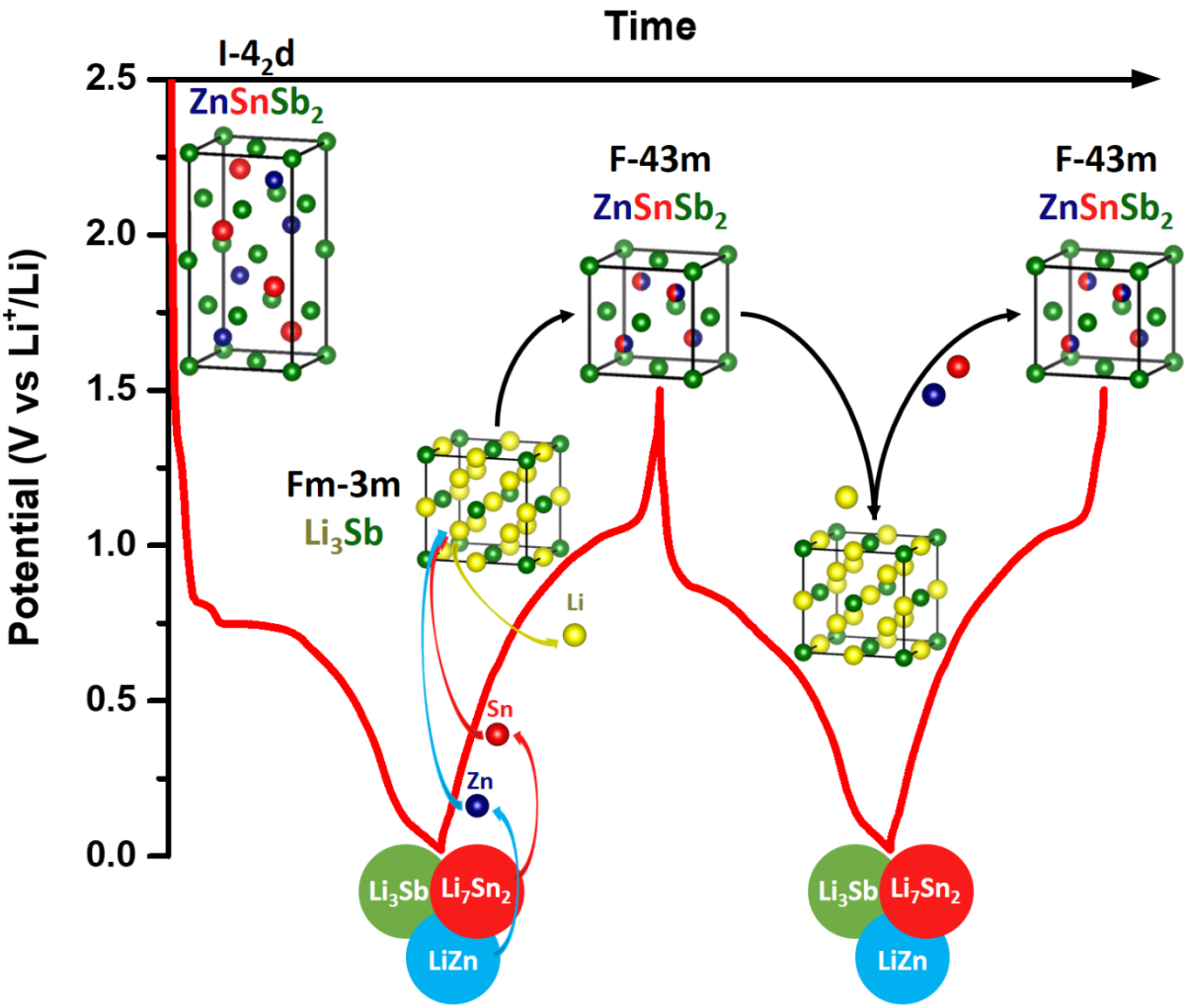
Time
I-4$_2$d
ZnSnSb$_2$
F-43m
ZnSnSb$_2$
F-43m
ZnSnSb$_2$
Fm-3m
Li$_3$Sb
Potential (V vs Li$^+$/Li)
2.5
2.0
1.5
1.0
0.5
0.0
Li
Sn
Zn
Li$_3$Sb
Li$_7$Sn$_2$
LiZn
Li$_3$Sb
Li$_7$Sn$_2$
LiZn

INTRODUCTION

The global world population growth induces greenhouse gas emission rise negatively contributing to global warming. The growing energy demands and the electrical device emergences require greener energy production development but also conversion and efficient storage systems. Developing high energy efficiency and long lifespan cells in Li-ion batteries (LIB) has become a crucial challenge.[1,2] Despite its limited theoretical capacities (C_{theo} = 372 mAh/g or 805 mAh/cm^3) and owing to its abundance and low cost, carbon graphite is still the best negative electrode material for Li-ion batteries. Nevertheless the need of new mature energetical electrodes can be required for some specific applications.

Sn-[3] and Sb-[4] based electrodes were extensively investigated due to their elevated densities and their availability to alloy with lithium, to form $Li_{4,4}Sn$ and Li_3Sb, providing high theoretical capacities (944 mAh/g / 7236 mAh/cm^3 and 660 mAh/g / 4409 mAh/cm^3, respectively). However, their main weakness is the large volume change (> 200 %) during the lithiation / delithiation processes, leading to the pulverization of the materials and the delamination of the electrode - current collector interphase inducing a poor cycling performance.[5] Two promising ways were proposed to tackle the volume expansion: the nanostructuration of the materials and the use of intermetallic alloys instead of a pure metal.[6,7] Using an intermetallic electrode involving an electrochemically non- (or a poorly-) active metal (generally among transition metals) can improve the capacity retention and the lifespan of the batteries. Indeed, the non-active metal acts as a buffer of the volume change and limits the electrode material pulverization, improving the cyclability. Among all transition and post-transition metals alloyed with Sn or Sb, some are active (Zn, Ag, Ge…)[8–10] and others are inactive (Fe, Ni, Cu…)[11–13] toward lithium. SnSb was widely studied and has proved to be a promising candidate for LIB. In fact, the non-

active metal free alloy SnSb exhibits a huge capacity retention of 700 mAh/g for 100 cycles before progressively fading.[14,15]

Many M_xSnSb ternary alloys with M an inactive transition metal were studied. Ru *et al.* prepared the $SnSbCu_x$/MCMB/carbon composite by multi-step synthesis method and showed a reversible capacity of 485 mAh/g after 100 cycles at a current density of 100 mA/g.[16] $Co_xSn_ySb_z$, reported by Ke *et al*. and synthetized by direct electrodeposition on a Cu nanoribbon, exhibited a capacity retention of 510 mAh/g over 150 cycles.[17] This high performance was explained by the existence of ultrafine pores in the Cu nanoribbons leading to a greater contact area between the active constituents and the current collector. Other previous works, on Ti (or Nb) -SnSb materials, synthetized by high energy ball-milling, led to a huge specific capacity up to 550 mAh/g after 250 cycles.[18,19] In this case, the high conversion mechanism reversibility was induced by metallic titanium (or niobium) nanoparticles formation during cycling.[20] Some ternary compounds composed by 3 active elements were also investigated. For instance, Zhang *et al.* prepared $SnSbAg_{0.1}$/RGO composite via chemical reduction and displayed a stable capacity up to 538 mAh/g after 200 cycles.[21] Liu *et al*. synthetized Zn_xSnSb/C composite nanofibers by electrospinning that exhibited a huge capacity retention of 663 mAh/g over 200 cycles.[22] Ge-Sn-Sb and Bi-Sn-Sb were also studied and showed interesting electrochemical properties for Na-ion batteries.[23,24] Generally, the ternary compounds $M_xSn_ySb_z$ reported in literature are composed by a mixture of binary alloys and not a single ternary phase.

To enhance the electrochemical properties of SnSb, we propose here to add zinc in the SnSb structure to form $ZnSnSb_2$ ternary phase. Zinc presents the advantages of abundance, low cost and to be active versus lithium. Moreover its low melting point and high electrical conductivity are advantages for the microwave synthesis and for the electrochemical performance

as electrode material in the battery, respectively. In the literature, $ZnSnSb_2$ chalcopyrite semiconductor was only studied for these structural[25,26] and thermoelectric properties.[27] This material is thus investigated for the first time as negative electrode for Li-ion batteries. Foremost, different synthesis ways (ball-milling, microwave, furnace) were explored. The electrochemical properties of the purest $ZnSnSb_2$ material were examined and an original lithium insertion / extraction mechanism was highlighted by *operando* X-ray diffraction.

EXPERIMENTAL SECTION

$ZnSnSb_2$ was synthetized by loading powders Zn (Alfa Aesar, -100 mesh, ≥ 99.9%) Sn (Aldrich, ≥ 99%) and Sb (Alfa Aesar, -325 mesh, 99.5%), with an atomic ratio 1:5:2 (Zn:Sn:Sb), in a vacuum sealed graphitized quartz tube. $ZnSnSb_2$ crystallizes only in a tin flux solution when a large excess of Sn is added. The ampule was then placed in a furnace and heated till 900°C during 12h with a ramp of 1°C/min. Afterward, the tube was firstly cooled to 350°C, kept at this temperature for 48h and secondly cooled to room temperature. The ampule was opened; the ingot with the large amount of Sn was recovered and crushed in an agate mortar. Then, the powder was placed in a beaker and the tin excess was removed by etching with concentrated HCl solution. Finally, crystallized $ZnSnSb_2$ was recuperated and washed two times with ethanol and acetone solutions.

Ball-milling synthesis method was performed by mixing Zn, Sn, and Sb in stoichiometric proportions (1:1:2) in a 3D high energy grinder (SPEX 8000 M). 8h and 16h of real milling time were carried out under argon atmosphere in a stainless steel jar containing 6 balls. The diameter of the stainless steel balls was 10 mm and the weight ratio between balls and powders was 46. $ZnSnSb_2$ was also synthetized using microwave route (MW)[14], details and XRD pattern are reported in supplementary information (Fig SI. 2).

The phase characterization was performed by powder X-ray diffraction (XRD) on a Philips X'Pert 2theta/omega diffractometer equipped with an X'Celerator detector and Cu $K\alpha_1$ radiation (λ = 1.510562 Å). Unit lattice parameters were obtained by profile matching refinement using FULLPROF software. The chemical tin environments were characterized by ^{119}Sn Mössbauer spectroscopy collected with a constant acceleration spectrometer employing a $Ca^{119m}SnO_3$ source. Scanning electron microscopy (SEM) was performed on a Hitachi S-4500 microscope equipped with an energy dispersive scattering (EDS) detector to describe the powder morphology.

Electrodes were prepared by mixing in a vial, $ZnSnSb_2$, carbon black (TIMCAL, Super P, BET = 62 m^2/g), vapor grown carbon fibers (Showa Denko, VGCF-H, BET = 15 m^2/g) and carboxymethyl cellulose (Aldrich, CMC, DS = 0.9, Mw = 250 000) with a weight ratio of 70:9:9:12 $\%_{wt}$ and adding deionized water as solvent. After 1 hour of stirring in a planetary ball-mill at 300 rpm, the obtained slurry was casted at 150 µm thickness on a copper foil (Goodfellow, 17.5 µm thick, 99.9%) and dried 24h at room temperature then 16h in a vacuum flask at 120°C to remove all the residual solvent. Finally, $ZnSnSb_2$ electrode loading was around 2 mg/cm^2 and the electrode porosity was estimated at 89%.

2032 Coin cells were assembled in an argon-filled glove box (0.5 ppm H_2O / O_2) using lithium metal as counter / reference electrode, a glass-fiber filter (GF/D, Whatman) separator soaked with 0.225 ml of the electrolyte solution and $ZnSnSb_2$ as working electrode material. The liquid electrolyte used was $LiPF_6$ 1M in PC:EC:3DMC (Solvionic, 99.9%) with a 1:1:3 vol. ratio and 5$\%_{vol}$ FEC (Aldrich, ≥ 98.5%) + 1$\%_{vol}$ VC (Alfa Aesar, ≥ 99%) as additives.

Electrochemical tests were carried out on a multichannel MTI system in galvanostatic mode from 0.02 to 1.5 V vs Li^+/Li at various C-rates (here, *C/n* rate means that one mole of lithium reacts with one mole of $ZnSnSb_2$ in *n* hours) and at room temperature. For the long time cycling,

the first discharge is realized at a *C/2* current density (i.e. 31.5 mA/g), followed by 48 hours of relaxation times. After this formation half cycle, cells were cycled at higher current up to *4C* (251.5 mA/g).

Operando XRD was performed on a self-supported $ZnSnSb_2$ electrode during the first cycle at *C/5* (i.e. 12.6 mA/g) in a specific cells with a beryllium window.[28] The XRD patterns were collected every 2 hours.

RESULTS AND DISCUSSION

Described in 1967 by Borshchevskii *et al*,[29] the ternary $ZnSnSb_2$ belongs to the semiconductor $A^{II}B^{IV}C_2^{V}$ compounds. In agreement with the literature, $ZnSnSb_2$ material can only be obtained through high-temperature melting with a large excess of Sn.[27,30,31] The stoichiometric reaction of Zn:Sn:Sb = 1:1:2 by high-temperature melting[27] or by high energy ball-milling (Fig. SI. 1), results in the formation of two binary alloys such as SnSb and ZnSb. In fact, the ratio Zn:Sn:Sb = 1:x:2 with x higher than 4 is essential to form a single-phase.[31] Here, Sn is used as a reactive flux and its excess can be then easily removed by etching with HCl solution. However the pure $ZnSnSb_2$, without any impurities is difficult to obtain because the phase crystallizes *via* a peritectic reaction at 360°C.

The XRD of $ZnSnSb_2$ powder on the angular domain 10 – 70 (2Θ°) is reported in Figure 1. The XRD pattern was analyzed and refined using Le Bail method. Crystallographic data give two possible structures for $ZnSnSb_2$, one crystallizing in the I-4_2d space group with lattice parameters a = b = 6.279(2) Å and c = 12.580(1) Å, and a second which crystallizes in *fcc* F-43m space group with lattice parameters a = 6.281(1) Å. In the tetragonal cell, Sb atoms are tetrahedrally coordinated by two Sn atoms and by two Zn atoms at a distance of 2.799 Å and 2.639 Å, respectively. The chalcopyrite crystallographic structure places Zn in position 4a (0, 0, 0), Sn in

4b (0, 0, 0.5) and Sb in site 8d (0.228, 0.25, 0.125). In the cubic blende cell Zn and Sn atoms share the same crystallographic 4a site (50/50). The *fcc* structure is built on $(Zn/Sn)Sb_4$ tetrahedra. Importantly, the differentiation between the chalcopyrite and the blende structure cannot be achieved by using classical powder diffraction techniques. In our case, $ZnSnSb_2$ crystallizes probably in the tetragonal structure because a specific reaction occurs during the first lithiation process, explaining later in the manuscript.

Furthermore, due to the synthesis method, a minor amount of SnSb was also detected by XRD. SEM pictures show aggregated particles composed of small grains, lower than 2 µm (inset Fig. 1b). ^{119}Sn Mössbauer spectroscopy was also performed to characterize the tin environments in $ZnSnSb_2$. The Mössbauer spectrum was collected at 25K to limit the temperature Lamb-Mössbauer factor influence and to quantify the tin alloy impurity (Fig. 1b).[32] The spectrum is fitted using two doublets. One to refine the $ZnSnSb_2$ environment with an isomer shift δ = 1.99(1) mm/s and a quadrupole splitting Δ = 0.27(2) mm/s and a second corresponding to SnSb impurity representing 15% of the absorption area, in agreement with the XRD analysis.

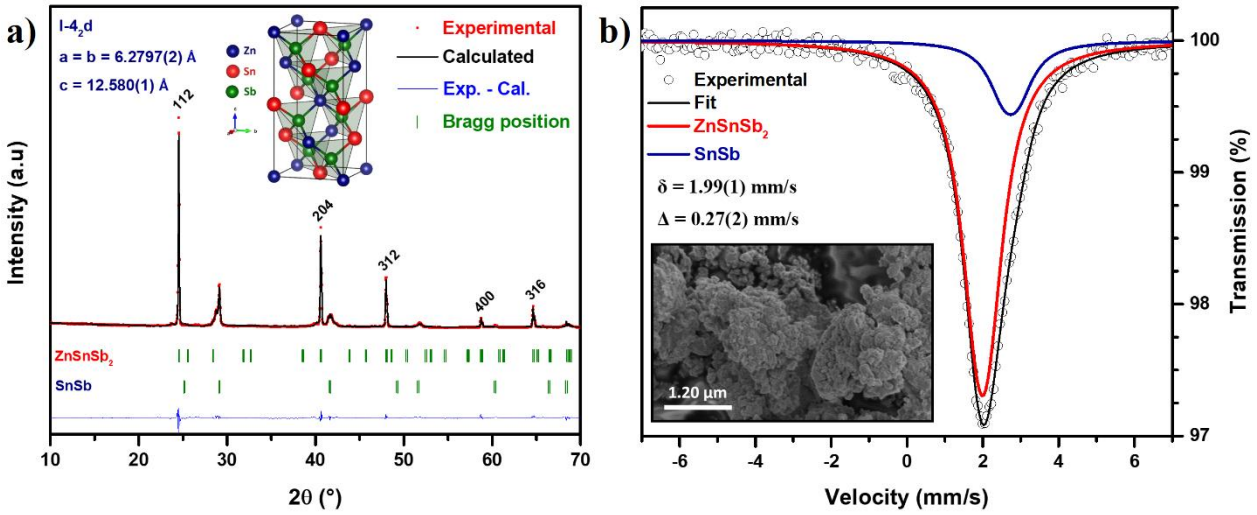

Figure 1: XRD pattern with the tetragonal chalcopyrite structure representation a), and ^{119}Sn Mössbauer spectrum at 25K with SEM picture b), of $ZnSnSb_2$ powder.

Figure 2 reports the electrochemical performance of $ZnSnSb_2$ electrode carried out in half-cell at room temperature. The initial discharge indicates two plateaus around 0.79 V and 0.73 V vs Li^+/Li before a gradually potential decrease down to 0.02 V (Fig. 2a). The electrode material reacts with 14 Li^+ offering a specific capacity of 880 mAh/g. During the following charge, no well-defined plateau clearly appears. A high reversible capacity of 730 mAh/g is obtained corresponding to a delithiation of 11.6 Li^+. The first cycle shows a coulombic efficiency of 83% which is relatively high, regarding the rapid charge current density of 251.5 mA/g. After three cycles, the specific capacity and the coulombic efficiency were stabilized around 635 mAh/g (3645 mAh/cm^3) and 99.6%, respectively. The experimental capacity is very close to the theoretical one (C_{theo} = 658 mAh/g or 3777 mAh/cm^3), if we consider the formation of LiZn, Li_7Sn_2 and Li_3Sb alloys in discharge. $ZnSnSb_2$ electrode displays a high cycling stability with 97% of the stabilized capacity and a coulombic efficiency up to 99.3% after 200 cycles (Fig. 2c). However, some capacity fluctuations were observed and can be explained by the cell temperature variations during the long cycling periods. We followed the battery polarization, which corresponds to the difference between the average potential in charge and discharge as function of the cycle number (Fig. 2d). During the first cycles, this polarization is 0.26 V and progressively increases until 0.34 V after 200 cycles. In fact, the average potential in charge was quite stable while in discharge it progressively drops. These results can suggest that the $ZnSnSb_2$ lithiation process becomes more difficult likely due to a thickening of the solid electrolyte interface (SEI) at the electrode surface produced by the decomposition of ethylene carbonate (EC) and $LiPF_6$ salt during the discharge.[33,34] Figure 2b presents the second cycle of the cyclic voltammogram of $ZnSnSb_2$ electrode recorded at 1 mV/s between 0.02 to 1.5 V vs Li^+/Li. Two

redox peaks couples at 0.62 / 0.27 V and 0.73 / 1.26 V appear in discharge / charge respectively, in agreement with the galvanostatic profile.

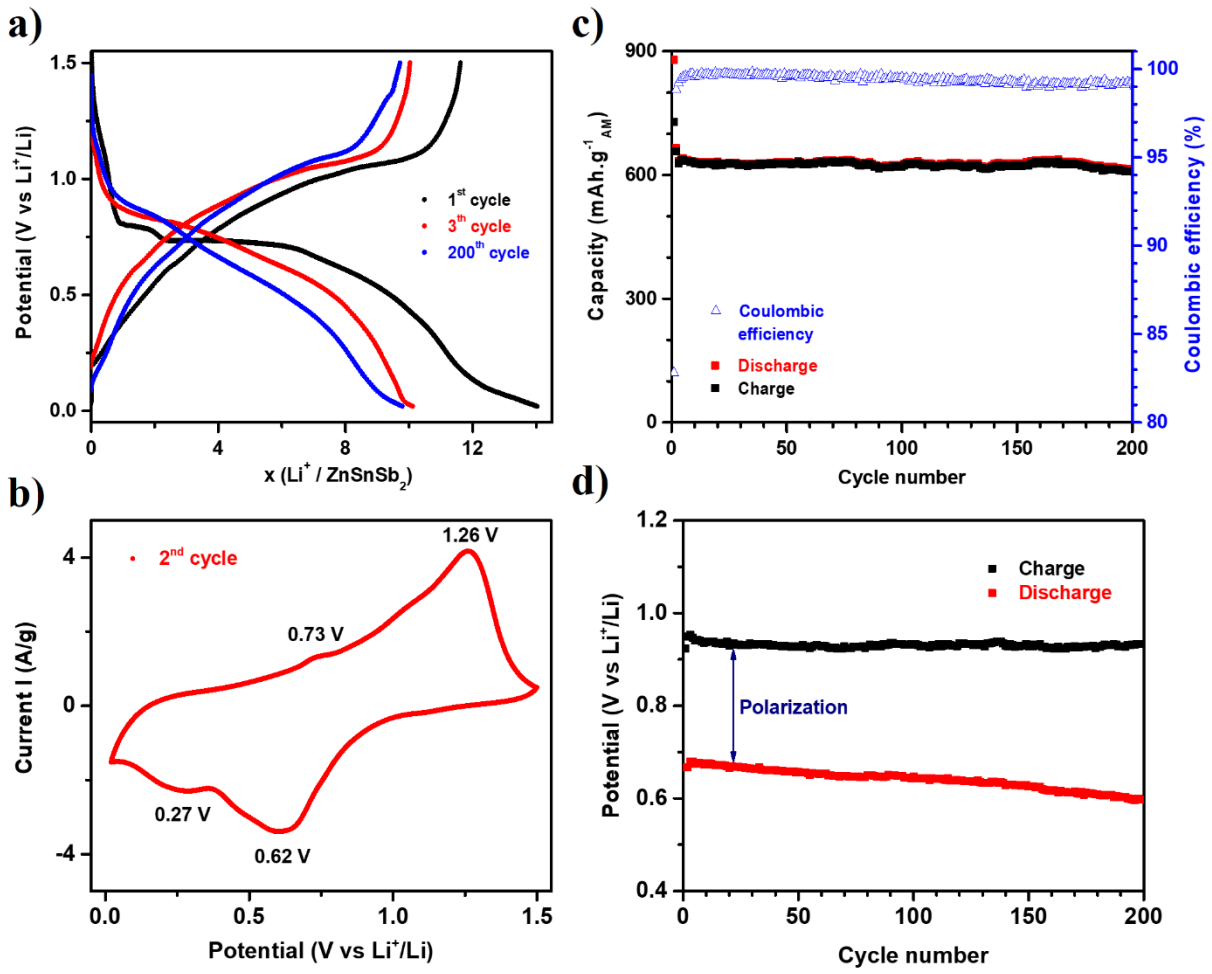

Figure 2: Galvanostatic profile a) and cyclic voltammetry b) of $ZnSnSb_2$ cycled between 0.02 and 1.5 V vs Li^+/Li. Specific capacity and coulombic efficiency c), average discharge/charge potentials d) as function of cycle number.

To further evaluate the electrochemical performance, $ZnSnSb_2$ electrode was cycled at various current rates from 12.6 mA/g (*C/5*) to 630 mA/g (*10C*) in the voltage range 0.02 – 1.5 V vs Li^+/Li. The rate capability was also presented in Figure 3. As expected, the specific capacity gradually declines when the current density increases. However, the loss of the initial capacity is limited to 19%, while current was multiplied by fifty (*C/5* to *10C*). It is noteworthy that the

capacity is much more stable after 30 cycles at various currents when a C-rate is applied again. $ZnSnSb_2$ material exhibited a huge capacity retention regardless to the current density, suggesting a high ability of the lithiation / delithiation processes and a great resistance to the mechanical stress of the electrode during cycling. To our knowledge, $ZnSnSb_2$ holds one of the best capability rates among MSnSb family of anode materials (Fig. SI. 3).[19,35–37] Note that the coulombic efficiency (CE) oscillates around 100% during the rate capability. Furthermore, a tiny increase of the cell polarization with the current density is observed from 0.11 V at *C/5* to 0.16 V at *10C*, showing a good electrode material tolerance for the lithium insertion / extraction (insert graphic on Fig. 3). Compared to TiSnSb and NbSnSb, $ZnSnSb_2$ exhibits a most outstanding rate capability and capacity retention over 200 cycles.[19,38]

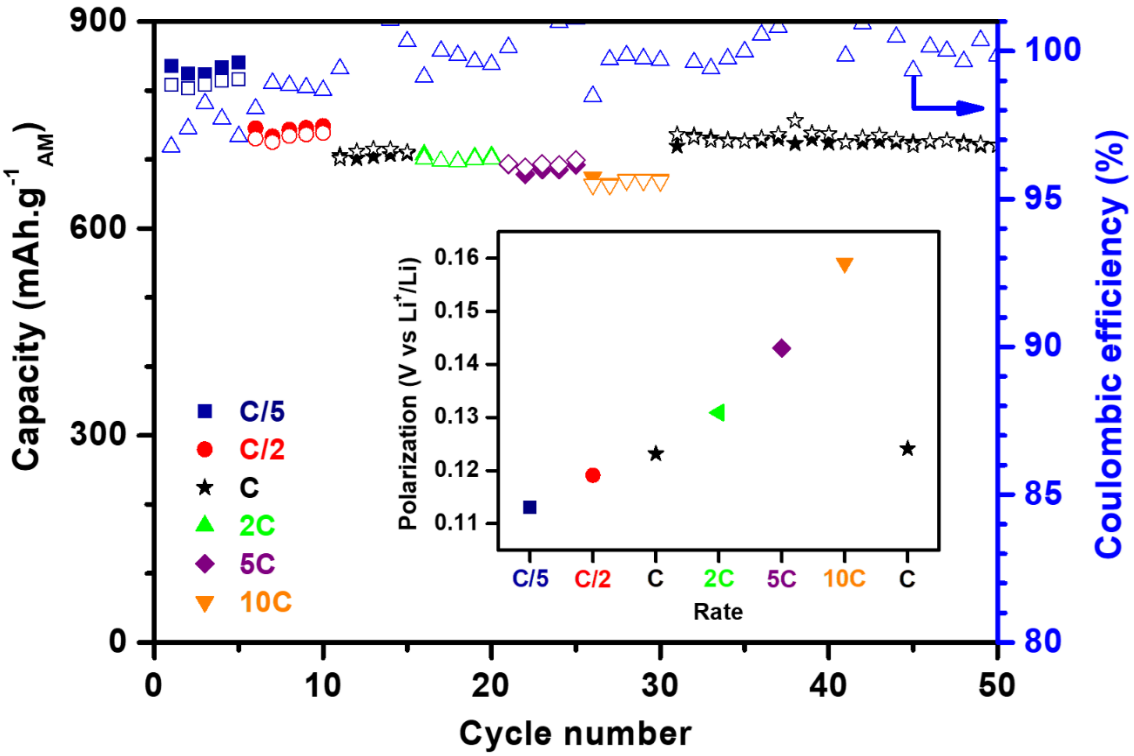

Figure 3: Rate capability and polarization (inset) of $ZnSnSb_2$ cycled at various current from C/5 to 10C between 0.02 to 1.5 V vs Li^+/Li at room temperature. (Filled: discharge; empty: charge).

Operando XRD measurement was performed on the first cycle of $ZnSnSb_2$ to get some information about the electrochemical reaction mechanism. Black and blue lines correspond to the XRD patterns collected during the first discharge and charge, respectively (right part of Fig. 4). The associated galvanostatic profile is shown on the left and the corresponding derivative curve is given in Fig. SI. 4. The XRD of the electrode at the OCV state revealed the well-defined crystalline peaks of $ZnSbSb_2$ at 24.5° and 40.5° which correspond to (112) and (204) of the tetragonal space group ((111) and (002) for the blende structure). The small impurities of SnSb appear at 29.1° and 41.8°. In order to get deeper information on the phase changes chronology, the Bragg peak areas evolution of each crystalline phase is reported as a function of time during the first discharge in Figure SI. 5.

First discharge. At the beginning of the lithium insertion reaction, $ZnSnSb_2$ Bragg peaks intensities remain constant suggesting that first lithium are consumed to form the solid electrolyte interphase (SEI), in agreement with literature reports.[33,39] Afterwards, SnSb impurities peaks progressively disappear from 0.81 V to 0.76 V and broad peaks appear at 23.5° / 26.7° / 38.6° and 30.6° / 32° / 43.8° / 44.9° corresponding to the cubic Li_3Sb phase (c-Li_3Sb) and β-Sn, respectively. The c-Li_3Sb refined structure cell indicates an Fm3m space group with lattice parameters a = 6.574(3) Å, close to the reported crystallographic data.[40] At 0.75 V SnSb is fully consumed and β-Sn diffraction peaks intensity stopped growing. Around the same potential, $ZnSnSb_2$ material starts to react with lithium and its Bragg peaks intensity gradually decreases until their total extinction at 0.66 V. Simultaneously c-Li_3Sb continues growing, while β-Sn does no more increase. During the last part of the first discharge, β-Sn is fully consumed and only the crystalline Li_3Sb continues growing until 0.50 V and then stays constant until 0 V.

As $ZnSnSb_2$ disappeared at 0.66 V and Li_3Sb continues to grow until 0.50 V, without any other new Bragg peaks appearance, suggesting that amorphous phase containing Sb is formed. In the lithiation of tin based electrode materials, the formed Li_xSn alloys are usually amorphous, and among them Li_7Sn_2 was the most common phase identified at the end of the discharge, in particular by Mössbauer spectroscopy.[41,42] On the other hand, Zn is also able to electrochemically form LiZn.[43,44] Nonetheless, the *operando* XRD does not allow to detect any Li_xSn or Li_yZn phases, likely due to the amorphous / nanoscale nature of the particles, rending the analysis difficult.

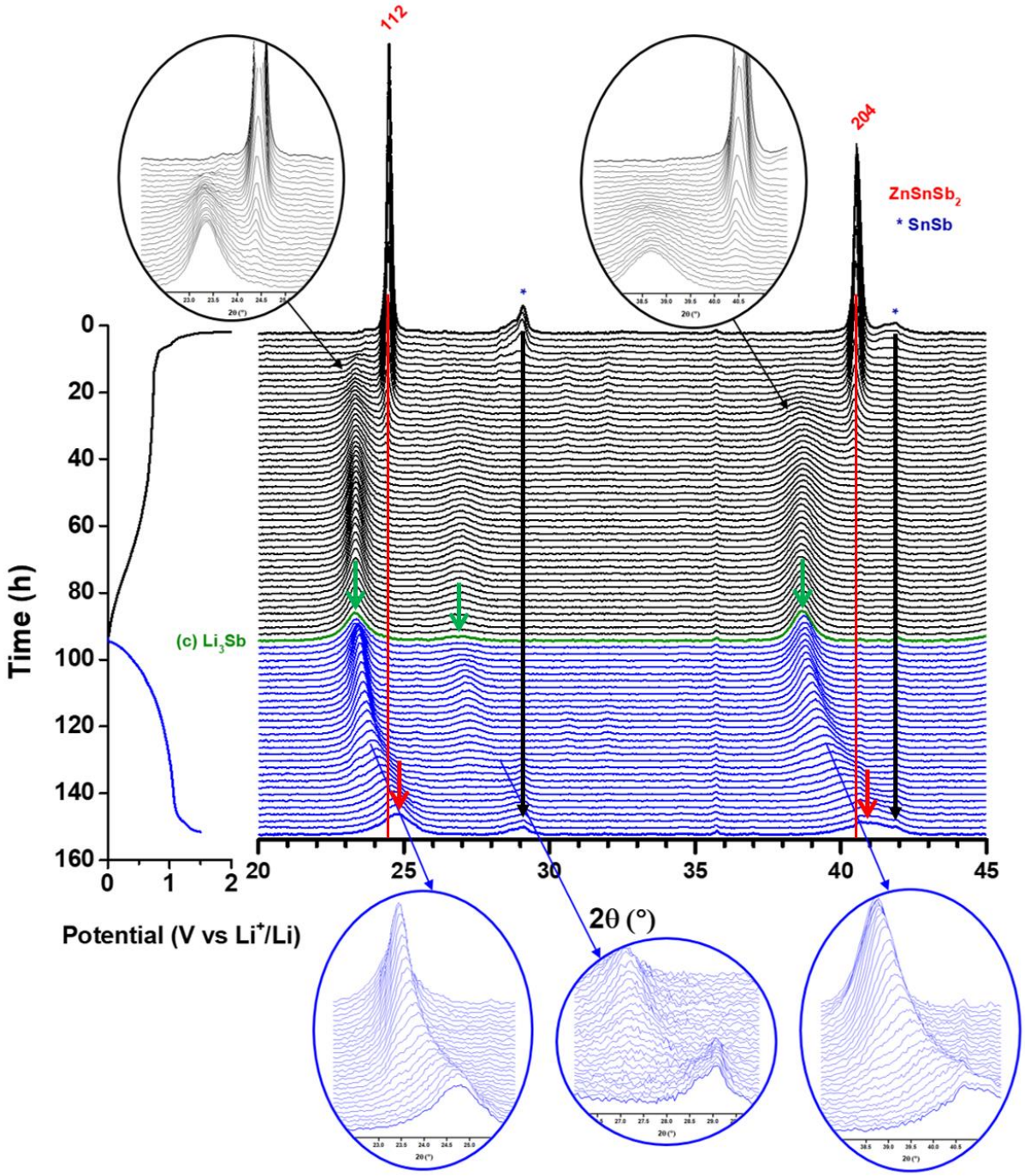

Figure 4: Operando XRD patterns collected during the first cycle of $ZnSnSb_2$ cycled between 0.02 to 1.5 V vs Li^+/Li at a C/5 rate at room temperature. Black and blue lines correspond to the first discharge and charge respectively. The green diffractogram represents the end of the discharge.

First charge. More interesting and surprising is the following charge of $ZnSnSb_2$. Initially, no change on the XRD patterns was observed during the delithiation processes suggesting that the amorphous tin and zinc lithiated phases formed at the end of discharge are firstly delithiated on charge. From 0.72 V to the end of charge, the c-Li_3Sb peaks at 23.5° and 38.6° shift toward higher 2Θ angles and go back to Bragg positions close to those of the $ZnSnSb_2$, while the one at 26.7° gradually disappears. Unlike the two-phase process identified in the first discharge, in charge this 2Θ shift of the Li_3Sb peaks indicates that a solid solution mechanism takes place during the delithiation. This solid solution is correlated with a decrease of lattice parameters of the *fcc* Li_3Sb phase. The two main broad Bragg peaks at the end of charge present the same angles than those of the pristine $ZnSnSb_2$ material (Fig. SI. 6). It is interesting to note that the *fcc* structure of $ZnSnSb_2$ presents a cubic lattice parameter (a = 6.281(1) Å) close to that of Li_3Sb (a = 6.559 Å).[30,40] Thus, it is suggested that the solid solution can be related to a progressive displacement reaction where Li are substituted in Li_3Sb by Sn and Zn atoms available from the delithiation of LiZn and Li_7Sn_2.[45] Note that the extremely broad peaks at the end of charge are likely due to the electrochemical grinding leading to amorphous / nanosized particles.

Finally, the $ZnSnSb_2$ electrochemical mechanism in Li-ion batteries is proposed Figure 5. As a biphasic reaction takes place during the first lithiation process, it can be suggested that the pristine material crystallizes in a tetragonal structure. Indeed if the pristine material crystallized in cubic structure, a solid solution (like in charge) should be expected. During the charge, a displacement mechanism occurs, suggesting that the lithium from Li_3Sb structure is progressively exchanged by Zn and Sn atoms to form the cubic $ZnSnSb_2$ in a *quasi-topotactic* reaction. Indeed, this singular solid solution / displacement de/lithiation mechanism could induce less volume

change during cycling leading to high capacity retention and explain the high tolerance of the electrode material at high current density.

It is noticeable that at the end of charge, the 29.1° and 41.8° peaks evidence the crystallization of SnSb and the good reversibility of its lithiation as previously reported in the literature.[46]

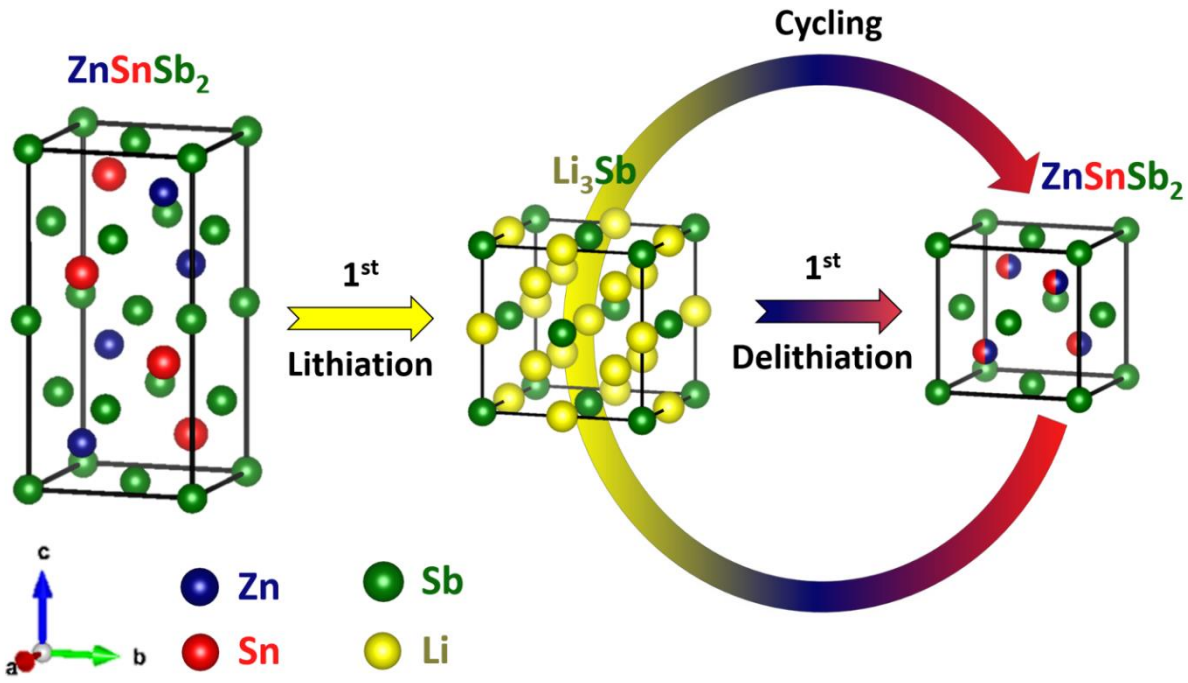

Figure 5: Electrochemical mechanism proposed for $ZnSnSb_2$ anode in Li-ion batteries.

CONCLUSION

This first study on $ZnSnSb_2$ negative electrode reports a singular reaction mechanism leading to high energy density and long lifespan for Li-ion batteries. Unlike all others ternary alloys containing Sn and Sb metals proposed as electrode material for LIB, $ZnSnSb_2$ is composed by three active elements inducing a higher theoretical gravimetric capacity (C_{theo} = 658 mAh/g). However, as the material grows only in a tin flux solution *via* a peritectic reaction which generates systematically tiny impurities, some optimization is required.

The electrochemical performance of the material synthesized at high temperature is very promising. Indeed, electrode material shows a capacity retention of 615 mAh/g after 200 cycles at a current density of 0.25 A/g with 99.3 % of coulombic efficiency. This result was not expected for a bulk micrometric material without any morphology optimization. Regarding the C-rate capability, $ZnSnSb_2$ electrode exhibits a better lithiation / delithiation ability at high current density (10C) compared to TiSnSb or NbSnSb.[19,35] This can be explained by the electrical conductivity of zinc which is higher than those of titanium or niobium and/or the particular mechanism.

In fact, o*perando* XRD measurement allowed highlighting two different lithiation / delithiation mechanisms during cycling. A biphasic reaction occurs during the first discharge while a solid solution / displacement reaction takes place during the following charge. This *quasi-topotactic* displacement reaction is facilitated by the crystallographic structures similarity of $ZnSnSb_2$ and Li_3Sb phases, and is obviously favorable to the high lithiation / delithiation processes reversibility inducing probably less degradation caused by volume change during cycling. Complementary characterizations, based on specific synchrotron radiation, will be needed to fully identify the electrochemical mechanism with the formation of supposed LiZn and Li_7Sn_2 phases.

ACKNOWLEDGMENTS

This research was performed in the framework of “Réseau sur le Stockage Electrochimique de l’Energie” (RS2E) and the ANR program no. ANR-10-LABX-76-01. Authors thank Total S.A. and ADEME for the financial support of G. Coquil’s PhD Thesis and also for the fruitful debates. Didier Cot from Institut Européen des Membranes (IEM) is also acknowledgments for SEM

pictures. Thanks to my colleges Aude Roland and Vincent Gabaudan for the helpful discussion and their encouragements.

There are no conflicts of interest to declare.

REFERENCE

1. Armand, M. & Tarascon, J.-M. Issues and challenges facing rechargeable lithium batteries. *Nature* **414**, 359–367 (2001).
2. Goodenough, J. B. & Park, K. The Li-Ion Rechargeable Battery : A Perspective. *J. Am. Chem. Soc.* (2013).
3. Ying, H. & Han, W.-Q. Metallic Sn-Based Anode Materials: Application in High-Performance Lithium-Ion and Sodium-Ion Batteries. *Adv. Sci.* **4**, 1700298 (2017).
4. He, J., Wei, Y., Zhai, T. & Li, H. Antimony-based materials as promising anodes for rechargeable lithium-ion and sodium-ion batteries. *Mater. Chem. Front.* **2**, 437–455 (2018).
5. Mukhopadhyay, A. & Sheldon, B. W. Deformation and stress in electrode materials for Li-ion batteries. *Prog. Mater. Sci.* **63**, 58–116 (2014).
6. Goriparti, S. *et al.* Review on recent progress of nanostructured anode materials for Li-ion batteries. *J. Power Sources* **257**, 421–443 (2014).
7. Cabana, J., Monconduit, L., Larcher, D. & Palacín, M. R. Beyond intercalation-based Li-ion batteries: The state of the art and challenges of electrode materials reacting through conversion reactions. *Adv. Mater.* **22**, 170–192 (2010).
8. Xu, J., Wu, H., Wang, F., Xia, Y. & Zheng, G. Zn4Sb3Nanotubes as Lithium Ion Battery Anodes with High Capacity and Cycling Stability. *Adv. Energy Mater.* **3**, 286–289 (2013).
9. Schmuelling, G. *et al.* Synthesis and electrochemical characterization of nano-sized Ag4Sn particles as anode material for lithium-ion batteries. *Electrochim. Acta* **196**, 597–602 (2016).
10. Fan, S. *et al.* Rapid fabrication of a novel Sn–Ge alloy: structure– property relationship and its enhanced lithium storage properties. *J. Mater. Chem. A* **1**, 14577–14585 (2013).
11. Wang, S. *et al.* Monodisperse CoSn2 and FeSn2 nanocrystals as high-performance anode materials for lithium-ion batteries. *Nanoscale* **10**, 6827–6831 (2018).

12. Liu, J., Wen, Y., van Aken, P. A., Maier, J. & Yu, Y. Facile Synthesis of Highly Porous Ni–Sn Intermetallic Microcages with Excellent Electrochemical Performance for Lithium and Sodium Storage. *Nano Lett.* **14**, 6387–6392 (2014).
13. Chen, J., Yang, L., Fang, S., Zhang, Z. & Hirano, S. I. Facile fabrication of graphene/Cu6Sn5 nanocomposite as the high performance anode material for lithium ion batteries. *Electrochim. Acta* **105**, 629–634 (2013).
14. Antitomaso, P. *et al.* Ultra-fast dry microwave preparation of SnSb used as negative electrode material for Li-ion batteries. *J. Power Sources* **325**, 346–350 (2016).
15. He, M., Kravchyk, K., Walter, M. & Kovalenko, M. V. Monodisperse antimony nanocrystals for high-rate li-ion and na-ion battery anodes: Nano versus bulk. *Nano Lett.* **14**, 1255–1262 (2014).
16. Ru, Q., Chen, X., Li, J., Guo, L. & Hu, S. The lamella SnSbCux/MCMB/carbon composite as high stability and durable anodes for lithium ion battery. *Electrochim. Acta* **193**, 180–190 (2016).
17. Ke, F. S. *et al.* Three-dimensional nanoarchitecture of Sn-Sb-Co alloy as an anode of lithium-ion batteries with excellent lithium storage performance. *J. Mater. Chem.* **22**, 17511–17517 (2012).
18. Marino, C. *et al.* Role of structure and interfaces in the performance of TiSnSb as an electrode for Li-ion batteries. *Chem. Mater.* **24**, 4735–4743 (2012).
19. Coquil, G. *et al.* On the high cycling stability of NbSnSb in Li-ion batteries at high temperature. *Electrochim. Acta* **281**, 619–623 (2018).
20. Fehse, M. *et al.* In-Depth Analysis of the Conversion Mechanism of TiSnSb vs Li by Operando Triple-Edge X-ray Absorption Spectroscopy: A Chemometric Approach. *Chem. Mater.* **29**, 10446–10454 (2017).
21. Zhang, P. *et al.* Influence of reduced graphene oxide on the morphology and electrochemical performance of SnSbAg0.1 composite materials. *Electrochim. Acta* **137**, 121–130 (2014).
22. Liu, L., Zhang, P., Li, Y., Ren, X. & Deng, L. Three-dimensional nanoarchitecture SnSbZn-C composite nanofibers as anode materials for lithium-ion batteries. *RSC Adv.* **6**, 52746–52753 (2016).
23. Farbod, B. *et al.* Anodes for sodium ion batteries based on tin-germanium-Antimony

alloys. *ACS Nano* **8**, 4415–4429 (2014).

24. Xie, H. *et al.* Sn-Bi-Sb alloys as anode materials for sodium ion batteries. *J. Mater. Chem. A* **5**, 9661–9670 (2017).
25. Shakra, A. M., Atyia, H. E. & Fadel, M. Single oscillator parameters and optical properties for ZnSnSb2 chalcopyrite in thin film form. *J. Alloys Compd.* **763**, 983–989 (2018).
26. Mishra, S. & Ganguli, B. Effect of p – d hybridization, structural distortion and cation electronegativity on electronic properties of ZnSnX2 (X = P, As, Sb) chalcopyrite semiconductors. *J. Solid State Chem.* **200**, 279–286 (2013).
27. Nomura, A. *et al.* Chalcopyrite ZnSnSb 2 : A Promising Thermoelectric Material. *ACS Appl. Mater. Interfaces* **10**, 43682–43690 (2018).
28. Leriche, J. B. *et al.* An Electrochemical Cell for Operando Study of Lithium Batteries Using Synchrotron Radiation. *J. Electrochem. Soc.* **157**, A606 (2010).
29. Borshchevskii, A. S., Goryunova, N. A., Kesamanly, F. P. & Nasledov, D. N. Semiconducting ABC2 Compounds. *Phys. Status Solidi* **21**, 9–55 (1967).
30. Scott, W. Preparation and some properties of ZnSnSb2. *J. Appl. Phys.* **44**, 5165–5166 (1973).
31. Tengå, A. *et al.* Sphalerite - Chalcopyrite polymorphism in semimetallic ZnSnSb. *Chem. Mater.* **17**, 6080–6085 (2005).
32. Sturhahn, W. & Chumakov, A. Lamb-Mössbauer factor and second-order Doppler shift from inelastic nuclear resonant absorption. *Hyperfine Interact.* **123**, 809–824 (1999).
33. Peled, E. & Menkin, S. Review—SEI: Past, Present and Future. *J. Electrochem. Soc.* **164**, A1703–A1719 (2017).
34. Wang, A., Kadam, S., Li, H., Shi, S. & Qi, Y. Review on modeling of the anode solid electrolyte interphase (SEI) for lithium-ion batteries. *npj Computational Materials* **4**, 15 (2018).
35. Wilhelm, H. A., Marino, C., Darwiche, A., Soudan, P. & Morcrette, M. Engineering study on TiSnSb-based composite negative electrode for Li-ion batteries. *J. Power Sources* **274**, 496–505 (2015).
36. Xia, X. *et al.* A simple method to encapsulate SnSb nanoparticles into hollow carbon nanofibers with superior lithium-ion storage capability. *J. Mater. Chem. A* **1**, 13807 (2013).

37. Fan, L., Liu, Y., Tamirat, A. G., Wang, Y. & Xia, Y. Synthesis of ZnSb@C microflower composites and their enhanced electrochemical performance for lithium-ion and sodium-ion batteries. *New J. Chem.* **41**, 13060–13066 (2017).
38. Madec, L., Gachot, G., Coquil, G., Martinez, H. & Monconduit, L. Toward efficient Li-ion cells at high temperatures: Example of TiSnSb material. *J. Power Sources* **391**, 51–58 (2018).
39. Balbuena, P. B. & Wang, Y. *Lithium-Ion Batteries : Solid-Electrolyte Interphase*. *Imperial College Press* (2004). doi:10.1142/p291
40. Brauer, G. & Zintl, E. Konstitution von Phosphiden, Arseniden, Antimoniden und Wismutiden des Lithiums, Natriums und Kaliums. *Zeitschrift für Phys. Chemie* **37B**, (2017).
41. Robert, F., Lippens, P. E., Olivier-fourcade, J., Jumas, J. & Gillot, F. Mössbauer spectra as a ‘“fingerprint”’ in tin–lithium compounds : Applications to Li-ion batteries. *J. Solid State Chem.* **c**, 339–348 (2007).
42. Chamas, M., Sougrati, M., Reibel, C. & Lippens, P. Quantitative Analysis of the Initial Restructuring Step of Nanostructured FeSn2-Based Anodes for Li-Ion Batteries. *Chem. Mater.* **25**, 2410–2420 (2013).
43. Zhao, X. B. & Cao, G. S. A study of Zn4Sb3 as a negative electrode for secondary lithium cells. *Electrochim. Acta* **46**, 891–896 (2001).
44. Park, C. M. & Sohn, H. J. Quasi-intercalation and facile amorphization in layered ZnSb for Li-ion batteries. *Adv. Mater.* **22**, 47–52 (2010).
45. Mauvernay, B., Doublet, M. L. & Monconduit, L. Redox mechanism in the binary transition metal phosphide Cu3P. *J. Phys. Chem. Solids* **67**, 1252–1257 (2006).
46. Antitomaso, P. *et al.* SnSb electrodes for Li-ion batteries: the electrochemical mechanism and capacity fading origins elucidated by using operando techniques. *J. Mater. Chem. A* **5**, 6546–6555 (2017).